



Viewpoints: Chemists on Chemistry

Anatomy of Elementary Chemical Reactions

Andrew J. Alexander and Richard N. Zare

Department of Chemistry, Stanford University, Stanford, CA 94305-5080

Anatomy of Elementary Chemical Reactions 1105

Outline

1. Introduction
2. Reaction Kinetics
3. Simple Collision Theory
4. Dissecting the Collision Process: Reaction Dynamics
5. Probing a Reaction
 - 5.1. The Chemist as Voyeur
 - 5.2. The Chemist as Sleuth
6. Crossed Molecular Beam Methods
7. Photoinitiated Bimolecular Reactions
 - 7.1. Concepts
 - 7.2. Machinery
 - 7.3. From a Molecular Point of View: The Center-of-Mass Frame
8. Photoinitiated Reactions: From Philosophy to Contemporary Practice
 - 8.1. Early Days
 - 8.2. Recent Experiments from our Laboratory
 - 8.2.1. The Reaction of Chlorine with Methane: Reagent Alignment
 - 8.2.2. The Reaction of Chlorine with Methane: Product Alignment
9. To the Future

1. Introduction

The alchemists of old sought the knowledge to transform one material to another—for example, base metals into gold—as a path to the elixir of life. As chemists have concerned themselves with the transformation from compound to compound, so they have become involved in trying to uncover the structures of molecules and the pathways that reactions follow. Classically, the study of reaction mechanisms in chemistry (1, 2) encompasses reaction kinetics, the study of velocities or rates of reactions, and reaction dynamics, the study of the nanoscopic motion and rearrangement of atoms during a reactive event. An essential aim of this article is to bring the reader to a favorable vantage point with a brief introduction to reactive dynamics (3–5), and from there to describe some examples of recent strategies that have been employed to promote a fundamental understanding of the anatomy of elementary chemical reactions. In the final section we ponder future directions for this rapidly evolving field of research.

Other Material on Chemical Kinetics in This Issue

Chemistry Time: Factors Affecting the Rate of a Chemical Reaction: JCE Classroom Activity #10	1120A	On the Meaning of K_m and V/K in Enzyme Kinetics	1153
		Dexter B. Northrop	
Excited State Lifetimes and Bimolecular Quenching of Iodine Vapor Giles Henderson, Ronald Tennis, Terry Ramsey	1139	The Quasi-Steady-State Approximation: Numerical Validation Richard A. B. Bond, Bice S. Martincigh, Janusz R. Mika, Reuben H. Simoyi	1158
The Reaction of a Food Colorant with Sodium Hypochlorite: A Student-Designed Kinetics Experiment Josefina Arce, Rosa Betancourt, Yamil Rivera, Joan Pijem	1142	Validity of the Quasi-Stationary-State Approximation in the Case of Two Successive Reversible First-Order Reactions V. Viossat and R. I. Ben-Aim	1165
A Simple Electrochemical Approach to Heterogeneous Reaction Kinetics K. J. Drok, I. M. Ritchie, G. P. Power	1145	Why the Arrhenius Equation Is Always in the “Exponentially Increasing” Region in Chemical Kinetic Studies Harvey F. Carroll	1186
A Student Experiment in Non-Isothermal Chemical Kinetics Steven C. Hodgson, Lawrence N. Ngeh, John D. Orbell, Stephen W. Bigger	1150		



Viewpoints: Chemists on Chemistry is supported by a grant from The Camille and Henry Dreyfus Foundation, Inc.

2. Reaction Kinetics

The first Nobel Prize (<http://nobelprizes.com/nobel/nobel.html>) for chemistry was awarded in 1901 to J. H. van't Hoff, who several years earlier had proposed relationships between the rates of a reaction and the concentrations of the species involved (6). Specifically, the rate of an elementary reaction of $A + B$ to yield products might have the form

$$-\frac{d[A]}{dt} = k(T)[A]^a[B]^b \quad (1)$$

where square brackets denote concentrations and the exponents a and b are often, but not always, integers (including zero). In eq 1, $-d[A]/dt$ is the rate of loss of the concentration of A, and $k(T)$ is defined as the rate constant, which is found to depend on temperature, T .

In 1889 the Swedish chemist Svante Arrhenius published his celebrated equation (6, 7),

$$k(T) = A \exp(-E_a/k_B T) \quad (2)$$

which expresses the sensitivity of the rate of a reaction as a function of temperature through the rate constant, $k(T)$. Equation 2 contains many hidden and subtle features. Molecules collide, as expressed by the pre-exponential factor A , which is related to the number of collisions per second, but reactions will occur only if collisions are sufficiently energetic. E_a is the activation energy, generally interpreted as the height of an energy barrier that must be surmounted, and $k_B T$ is the thermal energy at temperature T , where k_B is the Boltzmann constant. The exponential term is simply the fraction of collisions with sufficient energy to react.

3. Simple Collision Theory

Equation 2 is an empirical result culled from a number of observations of the overall rates of bulk macroscopic reactions. Numerous statistical models exist that attempt to derive or explain this result from first principles. The most basic of these is simple collision theory, which was first formulated in 1918 by W. C. McC. Lewis (8, 9). In simple collision theory, the reagents are treated as structureless spheres that do not interact until their internuclear separation, r , reaches some critical distance, d , as shown in Figure 1. The reaction is assumed to occur at $r = d$ if the component of the relative velocity along the line of centers of the colliding reagents is

sufficiently large to overcome some critical threshold energy, ϵ_0 . The component of the kinetic energy directed along the line of centers is

$$\epsilon_{lc} = \epsilon \left(1 - \frac{b^2}{d^2} \right) \quad (3)$$

In this equation, ϵ represents the collision energy of the system. The impact parameter, b , is a measure of the "closeness" of a collision (see Fig. 1): an impact parameter of zero represents a full head-on collision. As the impact parameter increases, the two reagents approach less closely and energy is increasingly directed into rotation about the center of mass of the collision system, that is, into centripetal energy. Hence, the fraction of energy along the line of centers decreases as b increases until a maximum impact parameter, b_{max} , is reached. At b_{max} , the energy along the line of centers is only just enough to surmount the reaction threshold energy, $\epsilon_{lc} = \epsilon_0$. At larger impact parameters, ϵ_{lc} is not large enough for reaction to occur. For $b \leq b_{max}$ the probability of reaction is unity, whereas for $b > b_{max}$ the probability of reaction is zero.

The cross section of the reaction as a function of energy is given by

$$\sigma(\epsilon) = \pi b_{max}^2 \left(1 - \frac{\epsilon_0}{\epsilon} \right) \quad (4)$$

for $\epsilon \geq \epsilon_0$. The cross section represents the target area (bull's-eye) for which reaction occurs: the larger the cross section, the more likely reaction will occur, and this is dependent on the kinetic energy of the colliding reagents, ϵ , and the threshold energy, ϵ_0 . An expression for the overall thermal rate coefficient, $k(T)$, may be obtained by integrating the product $\epsilon\sigma(\epsilon)$ over the thermal distribution of relative collision energies. The thermal distribution of collision energies is given by a Maxwell-Boltzmann distribution, and the calculation yields (9)

$$k_{sct}(T) = A_{hs}(T) e^{-\epsilon_0/k_B T} \quad (5)$$

with

$$A_{hs}(T) = \pi d^2 \left(\frac{8k_B T}{\pi \mu} \right)$$

$A_{hs}(T)$ is the rate of hard-sphere collisions, where

$$\mu = \frac{m_1 m_2}{(m_1 + m_2)}$$

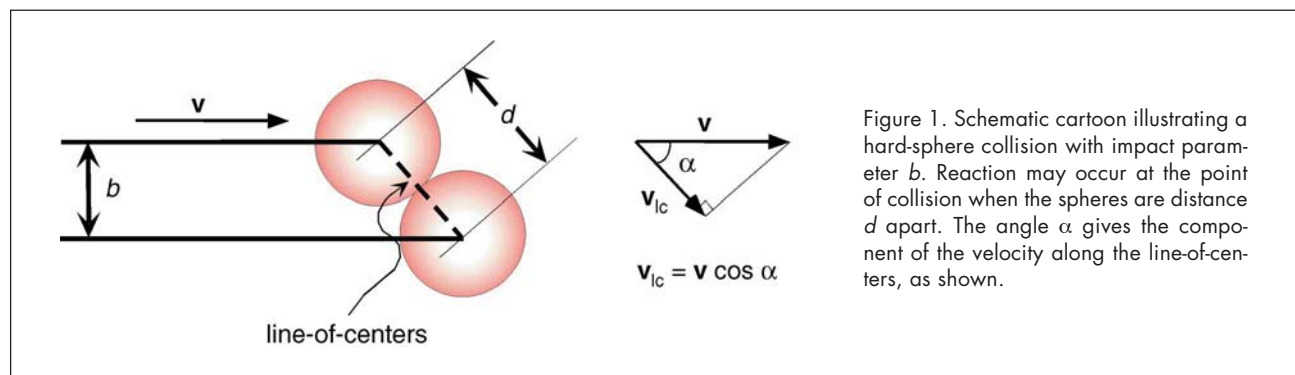
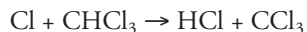


Figure 1. Schematic cartoon illustrating a hard-sphere collision with impact parameter b . Reaction may occur at the point of collision when the spheres are distance d apart. The angle α gives the component of the velocity along the line-of-centers, as shown.



is the reduced mass of the colliding reagents. It is clear that eq 5 has a similar form to eq 2, but the factor A now displays explicitly a dependence on temperature. One glaring assumption used in the derivation of eq 5 is that the reactants are structureless spheres: for example, the orientation of the reactant molecules when they collide has no influence upon the probability of reaction. This influence can be included in more advanced models (10) or by introducing an appropriate fudge factor (called the steric factor) to bring the result into agreement with experiment (2). For example, the reaction



at 300 K is found to be more than one hundred times *slower* than one would expect assuming a hard-sphere model. The small hydrogen atom is easily hidden by the bulky chlorine atoms of the CHCl_3 molecule and thus reduces the number of direct collisions of the Cl atom with the H–C bond.

4. Dissecting the Collision Process: Reaction Dynamics

The field of chemical dynamics involves the study of the motions of atoms as they interact and rearrange during a reactive encounter. The history of the field stretches back to the late 1930s, when the unfolding of quantum mechanics and a growing understanding of the nature of the chemical bond fostered the concept of the reactive potential energy surface (PES). The Born–Oppenheimer approximation assumes that the time scale for the motion of the nuclei is sufficiently slow for the electrons to rearrange at each nuclear configuration. This concept provides the basis for a microscopic picture of the rearrangement of atoms as motion over potential energy surfaces (3).

The PES represents the potential energy of the system as a function of nuclear configuration: a simple example of a PES for the hypothetical triatomic system (ABC) is shown in Figure 2. For the surface shown in Figure 2 we have assumed that the three atomic nuclei of the A–B–C system are restricted to a straight line (collinear), and we have plotted potential energy of the system as a function of the AB and BC bond lengths. The evolution of the reaction may be visualized as the motion of a single ball over this surface: as the ball rolls uphill kinetic energy is transferred into potential energy, as it rolls downhill potential energy is given into kinetic energy (11). The nuclear masses involved control the kinematic behavior. Features of the surface, such as minimum pathways and energy barriers, control the dynamic behavior of the nuclei. Together these factors govern all aspects of a chemical reaction. The number and nature of the available surfaces will strongly influence the reaction rate, the microscopic mechanism of the reaction, and the nature of the products formed. Surface topology will also determine the influences of reagent internal energy states on the reactivity.

The first study of the trajectories of atoms using classical mechanics was carried out as long ago as 1936 by Hirschfelder, Eyring, and Topley (12) on the hydrogen exchange reaction $\text{H} + \text{H}_2 \rightarrow \text{H}_2 + \text{H}$, using the potential energy surface of Eyring and Polanyi (13). Since then, the dynamics of numerous reactions have been interpreted using the concept of motion over one or more electronically *adiabatic* potential surfaces, valid within the bounds of the Born–Oppenheimer approxi-

mation. The prefixes *dia-* (from Greek “through”) and *adia-* (“not through”) stem from the type of functions used to represent potential energy surfaces and refer to the behavior (crossing or noncrossing) of these surfaces. A prime goal of reaction dynamics is to elucidate the nature of these surfaces and their effects on the motion of the nuclei (and electrons) as reactants are transformed into products.

Consider the simple gas-phase bimolecular reaction: $\text{A} + \text{BC} \rightarrow \text{AB} + \text{C}$. The rate constant and its variation with temperature are a unique indicator of the details of the reaction. Unfortunately we have here a nontrivial convolution of effects: in general, the reagents A and BC are populated in a range of internal energy states—vibrating and rotating with differing amounts of energy—and will collide with a range of velocities and at different orientations. To further complicate the understanding of this process the products can also populate a number of states: overall, the reaction explores numerous pathways. How can these effects be unraveled to give a clear picture of the making and breaking of bonds during a reactive encounter? For this purpose we must take some control over the reaction conditions by breaking thermal equilibrium (14).

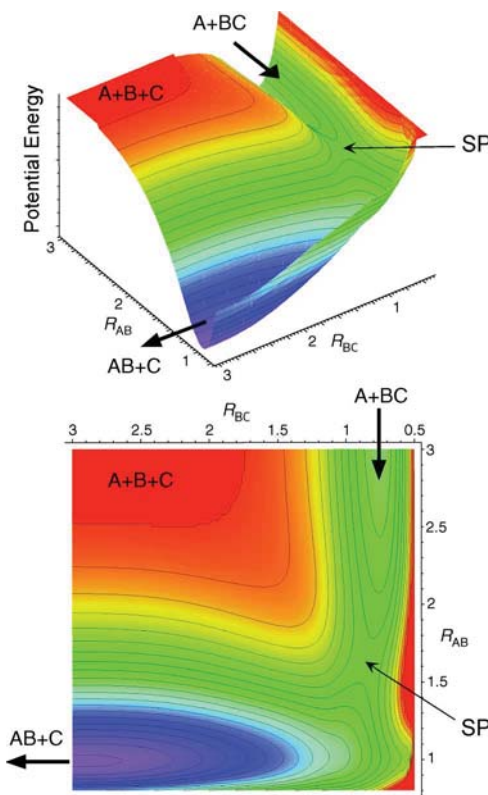


Figure 2. Two views of a hypothetical potential energy surface (PES) for the triatomic system A–B–C in a collinear geometry. R_{AB} and R_{BC} are the bond lengths (in Ångstrom units), the vertical coordinate is potential energy (arbitrary units). Note that, as shown, the reaction $\text{A} + \text{BC}$ is exoergic and has a barrier to the approach of the atom A, causing a “saddle point” (SP) in the entrance valley.

5. Probing a Reaction

5.1. The Chemist as Voyeur

The most direct approach to understanding an individual reaction is to watch it take place (15). Great progress has been made in this voyeuristic pursuit through use of ultrafast laser sources that produce pulses of light with picosecond (10^{-12}) and femtosecond (10^{-15}) duration. The technique of femtochemistry was pioneered by Zewail and colleagues at the California Institute of Technology (16). Such experiments are made possible by important technological advances, notably the development of femtosecond (fs) laser technology by Shank and coworkers in 1981 (17).

Figure 3 illustrates femtochemistry with the results of a study of curve crossing in sodium iodide (NaI). An initial femtosecond (pump) light pulse is used to excite NaI molecules to an excited PES (V_1 as shown in Fig. 3) and sets the

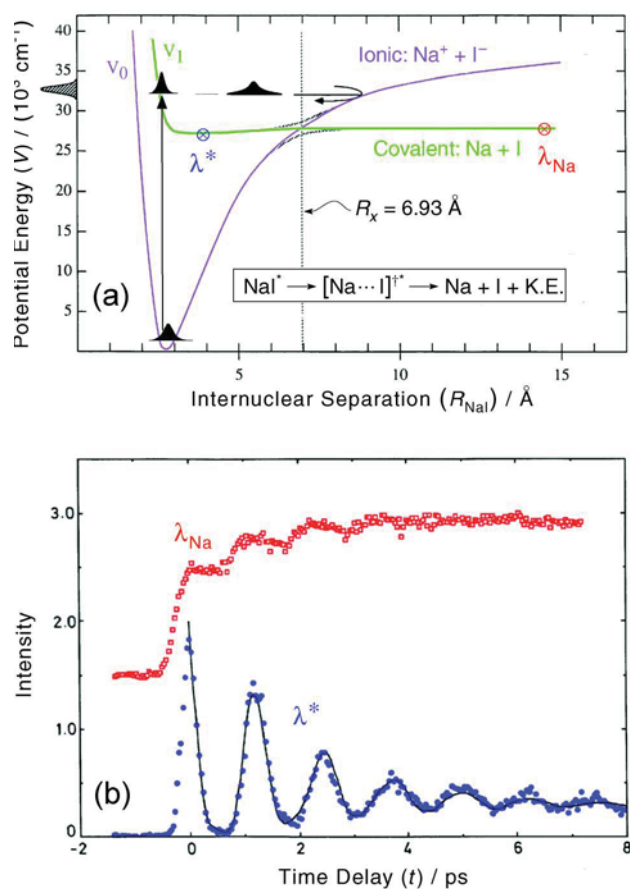


Figure 3. Wavepacket description of the photolysis of sodium iodide (NaI). (a) An fs pump light pulse excites ground state NaI molecules to an excited state wavepacket (arrow to black bell shape). Movement of the wavepacket corresponds to internuclear separation of the ensemble of NaI molecules. The wavepacket is interrogated by a second (probe) fs laser pulse, which is wavelength tuned to NaI absorption (λ^*) or to an absorption line of free Na atoms (λ_{Na}). The NaI absorption wavelength (λ^*) can be tuned to probe the wavepacket at various internuclear separations. The results are shown in (b). Red squares show subsequent accumulation of Na atoms at each wavepacket oscillation. Blue circles show the corresponding loss of NaI wavepacket. Time delay shown is the time delay for the probe pulse following the pump pulse. Figure adapted from ref 16.

“clock” at $t = 0$. The pump pulse creates a “wavepacket” of excited molecules that proceed to split apart: R_{NaI} increases as the molecules move down the potential energy slope. At a distance of $R_{\text{NaI}} = 6.93 \text{ \AA}$ the molecules encounter a curve crossing and some may “hop” from the covalent V_1 PES to the ionic V_0 PES. Some molecules continue to dissociate on V_1 and are lost; those molecules that hop to V_0 continue to higher R_{NaI} , but are eventually forced to return by the steep ionic potential energy slope. The wavepacket of NaI molecules can be probed as a function of time following the pump pulse using a second femtosecond (probe) laser pulse. The probe pulse can be tuned to look at either side of the crossing, by spectroscopy of the bound NaI molecules (at a wavelength λ^*), or of the free Na atoms (at a wavelength λ_{Na}) that escape and accumulate (see Fig. 3). The wavepacket oscillates back and forth several times in the well formed by the covalent and ionic surfaces, and a small fraction is lost at each oscillation (18).

Although the femtochemistry approach is conceptually appealing, it is clouded by the need to connect *spectroscopically* the state being probed to some other state throughout the reagents’ act of intimate entanglement. Consequently, the interpretation of such data may be hindered by lack of knowledge of loosely bound systems. An alternative approach is to look before and after the reaction and reason what has happened in between.

5.2. The Chemist as Sleuth

An intuitive method of probing the region of molecular interaction in a reactive encounter is to look at the aftermath of the reaction by spectroscopy of the products, provided that experimental conditions (low pressures) are chosen so that other collisions do not interfere. Two types of information can be gained in this way: scalar and vector. Scalar information relates to the magnitudes of properties—for example, the amount of energy distributed into translation, rotation, and vibration (19). Vector information necessarily includes a sense of direction in properties of interest, such as the polarization of the product’s rotational angular momentum vector, \mathbf{J}' , which can indicate to us if and how molecules prefer to rotate as they leave the reaction. Observation of the \mathbf{J}' vector lends us clues to the *angular* forces (torques) that fragments are subjected to during the reaction process. Another vector quantity is the correlation between the product and reagent relative velocity vectors, \mathbf{k}' and \mathbf{k} , which provides information on the *linear* forces at play during the reaction process. Together, these vector distributions contain a subtle yet powerful snapshot of the anatomy of a reaction process (see Fig. 4).

The correlation between the \mathbf{k}' and \mathbf{k} vectors can be conveniently presented as a velocity-angle scattering map. A typical polar map is reproduced in Figure 5 for the $\text{F} + \text{H}_2$ reaction (20). How was this map obtained and what does it describe?

6. Crossed-Molecular-Beam Methods

The molecular-beam method was introduced in the early 1950s and involves the creation of fast streams of atoms that can then react with target molecules (21–23). Because the beams formed are dilute, collisions within the beam are negligible. Two beams are made to intersect in a vacuum, and the direction and velocity of the product molecules ejected from the collision zone are measured. The first experiments

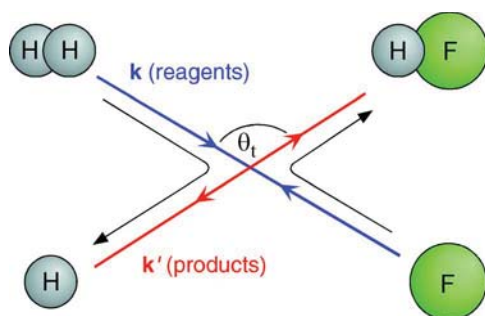


Figure 4. A schematic of a reactive scattering event for the reaction $F + H_2 \rightarrow HF + H$ showing the correlation between the relative velocities of the reagents (\mathbf{k}) and products (\mathbf{k}'). In this example, the products are scattered nearly sideways ($\theta_t \approx 90^\circ$) with respect to the F atom reagent.

using crossed pairs of beams were limited to a special family of reactions that yield very high fluxes of readily detectable product molecules: namely, the reactions of alkali metal atoms with halogen-containing target molecules. The product alkali halide salt was detected using surface ionization on a hot filament. Because these reactions were widely studied in the 1960s the period has been nicknamed the “alkali age” of reaction dynamics. The crossed-beam method blossomed in the 1970s with the development of “universal machines” that used for a detector a mass spectrometer that could be rotated with respect to the fixed-beam sources (23, 24). A typical chamber is illustrated schematically in Figure 6. By the 1980s, crossed-beam studies had matured sufficiently to allow Y. T. Lee and coworkers to produce a beautifully detailed experimental study of the reaction of $F + H_2$, a reaction that has become a benchmark in the field of reaction dynamics (25). The mass spectrometer is rather insensitive to the internal state of the product, but the kinematics of the $F + H_2$ system enabled the vibrational resolution of the angular scattering of the HF products, as illustrated in Figure 5. The relative masses of the H and F atom, the large vibrational energy spacing in the HF product, and the low product rotation all contributed to the fortuitous resolution of vibrational states according to the range of product speeds.

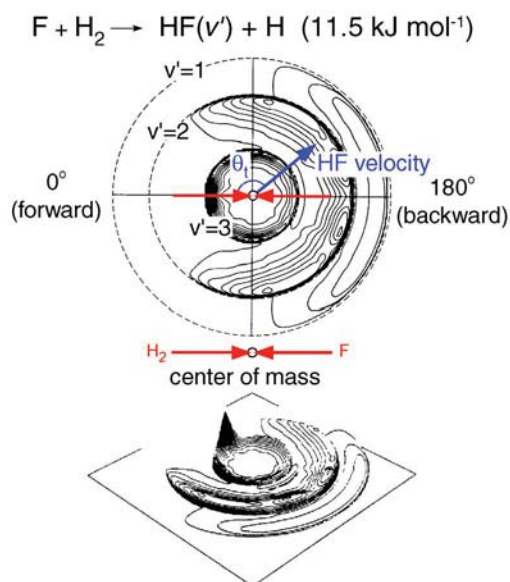


Figure 5. Velocity-angle polar map showing the distribution of $HF(v')$ products as a function of the CM scattering angle, θ_t . The dashed circles represent the maximum attainable velocities for each product internal state; products with higher internal energy are born with lower translational energies (innermost velocity circles). Zero degrees (0°) represents forward scattering with respect to the approach of the F atom reagent. Figure reproduced (adapted) with permission from ref 20 (copyright 1985 American Institute of Physics).

Figure 5 has become a unique and striking icon for reaction dynamicists. The polar map shows the amount of HF products scattered in various directions relative to the direction of the incoming F atom (see also Fig. 4). The center point of the polar map represents the center of mass (CM) of the system, and the radial coordinate indicates the velocity of the HF products: the further from the center, the faster the HF products are traveling. The CM defines the reagents' frame of reference for the collision, and is the natural coordinate system to use to describe the reaction. Another relevant frame of reference is the laboratory or LAB frame, from which we view the collision as outside observers (1). The transformation

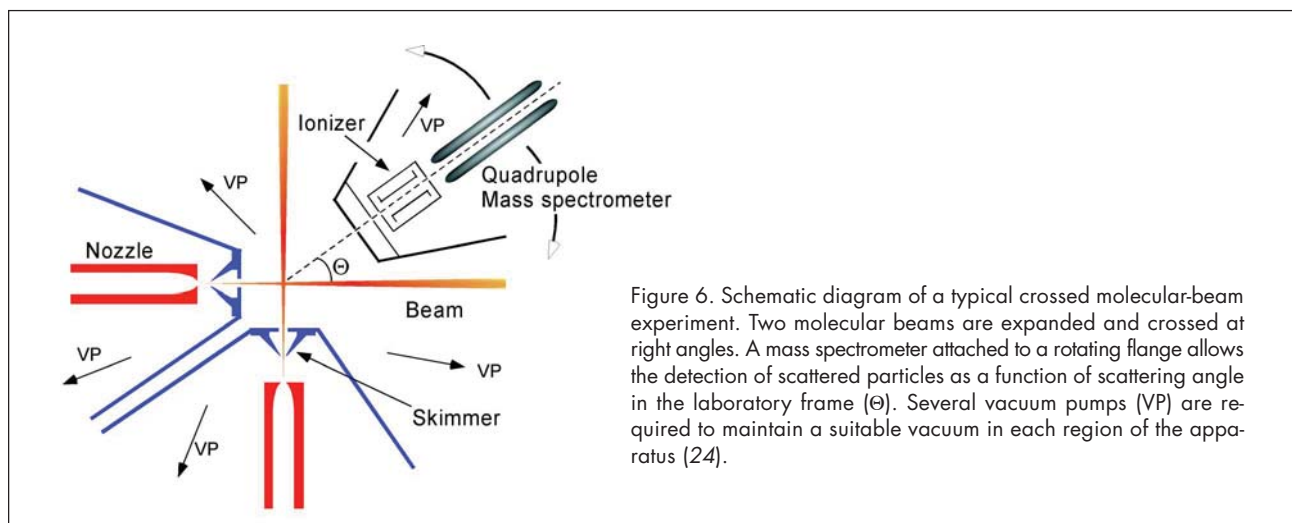


Figure 6. Schematic diagram of a typical crossed molecular-beam experiment. Two molecular beams are expanded and crossed at right angles. A mass spectrometer attached to a rotating flange allows the detection of scattered particles as a function of scattering angle in the laboratory frame (θ). Several vacuum pumps (VP) are required to maintain a suitable vacuum in each region of the apparatus (24).

between the CM and LAB frames will be discussed further in section 7.2.

As can be seen in Figure 5, the products are preferentially born in higher vibrational levels (peaking at $v' = 2$) and are mostly scattered backward with respect to the incoming F atom. Note also the change from backward to forward scattering for the highest energetically accessible level, $v' = 3$. This subtle change would have been hidden if the HF products had not been resolved according to their vibrational energy. The occurrence of forward scattering for HF($v' = 3$) has taken more than a decade to understand and has stimulated some of the most thorough theoretical work in the field. The backward scattering and product energy disposal were suggestive of a mechanism in which the F atom attacks one of the H atoms directly: a high-energy release early in the collision trajectory causes H and F to pull together rapidly, creating high product vibration. Initially, the forward scattering was taken as indicative of quantum mechanical "resonances": the HHF was thought to persist long enough to allow the molecule to rotate by about 180° . A mixture of this "indirect" mechanism was generally believed to lead to the shifting of the "direct" backward-scattering mechanism to forward-scattering for HF($v' = 3$). More recent experimental work, which directly probes the F + H₂ transition state region, and increasingly high-level ab initio calculations of the potential energy surface have forced a revision of this interpretation (25). The new results indicate that it is the precise shape of the PES in the transition state region that is responsible for the forward scattering. A similar situation has been observed in the reaction of chlorine atoms with methane (see section 8.2). Finally, it has been suggested that effects of quantum resonances in this reaction may yet be observed (26) but will require higher resolution of product speeds.

Product vibrational state resolution represents a step nearer the goal of unraveling reaction dynamics. For the majority of reactions, however, the spread in velocities between different product internal states is not sufficiently wide to allow internal state resolution by means of the crossed-molecular-beam method. In some cases, the mass combination or energetics of the reaction makes it difficult to obtain full angular resolution. Added to this difficulty is the challenge inherent in the low product flux, which results from collisions between two dilute molecular beams. Alternative strategies are sometimes available to overcome these drawbacks. We turn our attention to these strategies.

7. Photoinitiated Bimolecular Reactions

7.1. Concepts

One alternative strategy to the crossed-beam method substitutes the rotating mass spectrometer with optical detection of the products at the collision zone and makes use of tunable laser sources to initiate and probe the reaction. The flash photolysis method was introduced in the early 1950s by Porter and Norrish (6, 27) as a way to measure the rates of reaction on a microsecond time scale. The flash-photolysis method is akin in principle to high-speed photography (see Fig. 7). Reagents are allowed to flow through the reaction chamber, and the reaction is initiated by a flash of intense radiation from a flashlamp. Another flashlamp is used to measure the absorption spectrum of the products. The flash photolysis techniques provided the first direct evidence for the

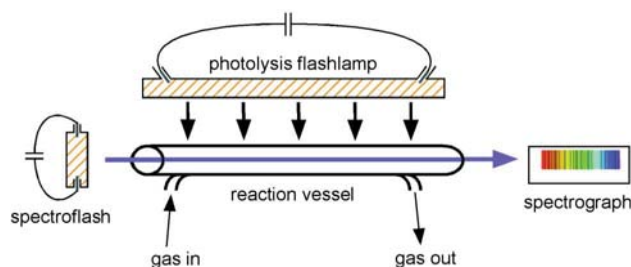
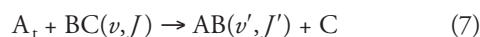


Figure 7. The principle of flash photolysis. A gas mixture flows into the reaction vessel, and reactions are initiated by a burst of intense radiation from a flashlamp. A second flashlamp acts as a source for measurement of the absorption spectrum of the resultant gas mixture.

existence of free radicals. As lasers became available in the 1960s, the time scale for measuring reactions was significantly reduced (16), and the flash photolysis technique gave birth to many others, particularly femtochemistry (section 5.1).

7.2. Machinery

Consider the hypothetical photoinitiated reaction sequence



where AD is the precursor molecule and BC the target molecule that is populated in a range of vibrational-rotational states, denoted (v, J) . Linearly polarized laser light dissociates AD molecules, producing a pulse of fast (translationally "hot") atoms, denoted A_t , whose velocities are aligned with respect to the polarization vector of the light.

The fast A_t atoms react with the target molecules and the products are given little time to build up, typically only a few tens of nanoseconds, so as to avoid collisions with other fragments. AB product molecules are detected selectively in vibrational-rotational states (v', J') using a second laser (the "probe" laser). In order to determine the angular scattering of the products, this final step must be sensitive to the velocity distribution of the products. A typical method for achieving this sensitivity is multiphoton ionization (MPI) coupled with time-of-flight (TOF) mass spectrometry. The second laser source is tuned to ionize AB molecules selectively from specific vibrational-rotational states (v', J') , and the time distribution for the AB^+ ions to reach a remote detector is related to their initial velocity distribution (see Fig. 8). An alternative method is to employ the Doppler effect: products moving toward (or away from) the probe laser detection axis show a blue (or red) shift in their absorption spectrum. The Doppler-broadened shape of the absorption feature is sensitive to the product's velocity distribution.

7.3. From a Molecular Point of View: The Center-of-Mass Frame

The measurements illustrated in Figure 8 represent a core slice of the product's velocity in the LAB frame. The product distribution is determined by the dynamics of the collision in the frame of the molecules; that is, only the relative velocity of the reagents is important. The relative velocity of the reagents is referenced to the center-of-mass (CM) frame of

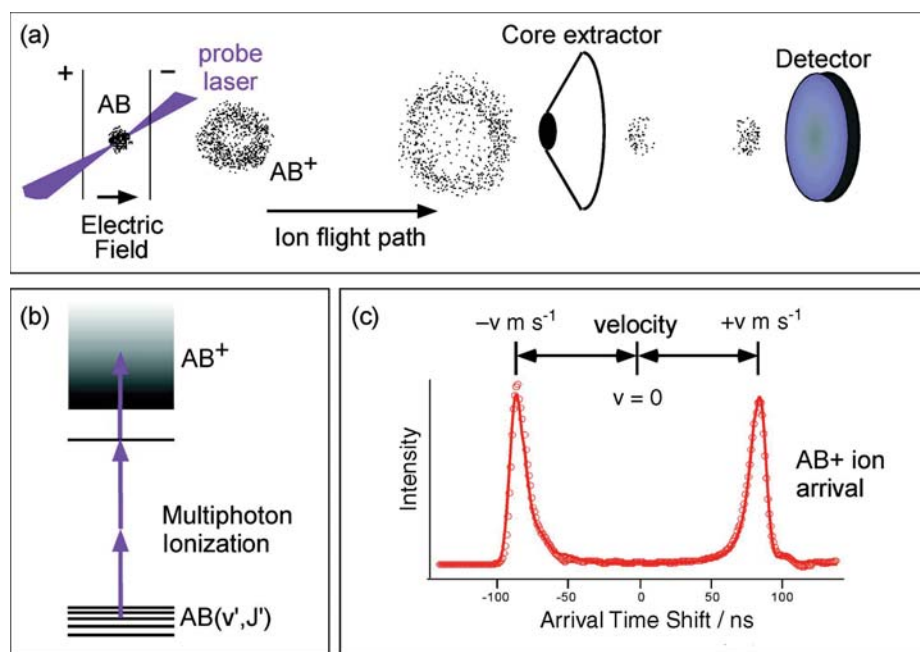


Figure 8. (a) Principles of the TOF method showing a measurement of AB molecules from the hypothetical reaction $A + BC \rightarrow AB + C$. The AB molecules are ionized by tuning the probe laser to excite a specific vibrational-rotational level (v', J') and the packet of ions continues to expand as a result of the initial velocities imparted to the AB molecules from the reaction. The whole ion packet is forced along a flight tube by means of an electric field, and a core is taken through the ion packet by use of a mask placed before the detector (28). The method of ionization, by absorption of 3 photons, is shown schematically in (b). A sample result is shown in (c): red circles are experimental points, solid line is a simulated fit to the data. The velocities of the product molecules can be determined from the spread between arrival times.

the system. If the target molecule is near stationary, the velocity of the center of mass, \mathbf{v}_{cm} , will be

$$\mathbf{v}_{\text{cm}} = \left[\frac{m_A}{m_A + m_{BC}} \right] \mathbf{v}_A \quad (8)$$

where \mathbf{v}_A is the LAB velocity of A (boldface denotes a vector quantity). Note that \mathbf{v}_{cm} is not available as energy to the colliding reagents for the reaction, only their relative velocity (\mathbf{k}') is available as collision energy. A simplified velocity vector diagram (which may be called a collapsed Newton diagram) for a reactive collision is shown in Figure 9, where the target velocity, \mathbf{v}_{BC} , is 0. The LAB frame velocities of products AB (or C) scattered at an angle θ_t and with velocities \mathbf{u}_{AB} (or \mathbf{u}_C) in the CM frame will be

$$\mathbf{v}_{AB} = \mathbf{v}_{\text{CM}} + \mathbf{u}_{AB} \quad (9)$$

For the forward-scattered products, $\theta_t \rightarrow 0^\circ$ and their LAB speed is enhanced by $|\mathbf{u}_{AB}|$; for backward-scattered products, $\theta_t \rightarrow 180^\circ$ and their LAB speed will be diminished by $|\mathbf{u}_{AB}|$. The simple vector sum (eq 9) provides a means of determining the angular distribution of \mathbf{k}' with respect to \mathbf{k} by measuring the distribution of LAB speeds $|\mathbf{v}_{AB}|$. The sensitivity is maximized when $|\mathbf{v}_{\text{CM}}| = |\mathbf{u}_{AB}|$ (or $|\mathbf{u}_C|$).

By the law of cosines

$$|\mathbf{v}_{AB}|^2 = |\mathbf{v}_{\text{CM}}|^2 + |\mathbf{u}_{AB}|^2 + 2|\mathbf{v}_{\text{CM}}||\mathbf{u}_{AB}|\cos\theta_t \quad (10)$$

If we assume that the partner fragment C carries away no internal energy, and if we know, or can reasonably estimate,

- the speed distribution of reagents A,
- the internal energy of BC, and
- the reaction exoergicity (i.e., the energy release),

then fixing the product quantum state (v', J') will fix the kinetic energy of the scattered products and therefore the speed $|\mathbf{u}_{AB}(v', J')|$. In these idealized conditions each laboratory speed $|\mathbf{v}_{AB}(v', J')|$ maps onto a center-of-mass scattering angle, θ_t , and the family of LAB speeds provides a snapshot of the

angular distribution of state-selected products in the molecular (CM) frame (29, 30).

These idealized conditions are not practically attainable, and a certain degree of averaging over any of the above will introduce a degree of blurring into the experimental results. Fortunately, this blurring can be accommodated to some extent in the modeling or minimized by judicious choice of experimental conditions. The thermal spread of velocities in the reagent source and the molecular target, as well as thermal population of their internal quantum states, can be reduced by expanding the reagents as a dilute solution in an inert carrier gas, such as helium, through a pinhole into a high vacuum. Alternatively, specific reagent quantum states can be selected by optical excitation, as we shall see in section 8.2. It is convenient to give the class of experiments of this type a name (31, 32); we call them *photoloc experiments*, for “photoinitiated bimolecular reactions using the law of cosines.”

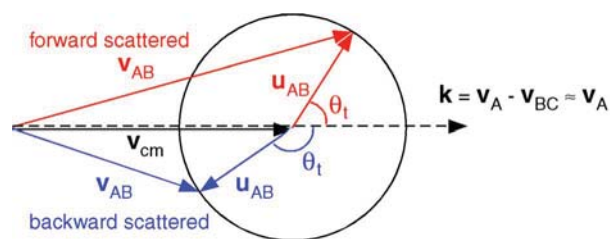


Figure 9. A simplified velocity vector diagram (collapsed “Newton” diagram) for the simplified case mentioned in the text. For clarity, a single product speed $|\mathbf{u}_{AB}|$ in the molecular (center-of-mass) frame is indicated. A more complicated figure would use the relative velocity vectors \mathbf{k} and \mathbf{k}' of the reagents and products. The magnitude of the velocity vector $|\mathbf{v}_{AB}|$ as measured in the laboratory (LAB) frame depends on the *direction* of motion of AB in the center-of-mass frame. The reader is invited to imagine different situations where the speed of AB $|\mathbf{u}_{AB}|$ or of the center-of-mass $|\mathbf{v}_{\text{CM}}|$ is smaller or larger and how this would affect the measurement of $|\mathbf{v}_{AB}|$ for different scattering angles.

8. Photoinitiated Reactions: From Philosophy to Contemporary Practice

8.1. Early Days

As we have intimated above, the use of polarized photolysis of a precursor to produce a reagent “beam in a bulb” is a powerful method that allows state-resolved detection of the reaction products at the collision center. The philosophy is well illustrated by one of the pioneering experiments done in this way (33), in the laboratory of Richard Bersohn, Columbia University. Hydrogen atoms were generated by polarized photodissociation of the precursor H_2S :



The hydrogen atoms reacted with deuterated silane (SiD_4) as the target molecule, to replace one of the D atoms with

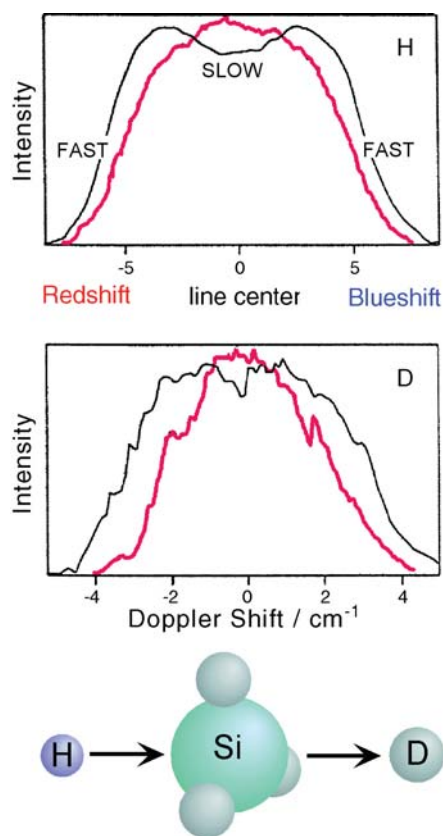
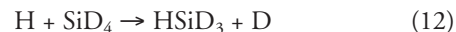


Figure 10. Experimental results from a study of the reaction of $\text{H} + \text{SiD}_4$. Top graph: Doppler measurement of the reagent H atoms; lower graph: Doppler measurement of product D atoms. The horizontal axis measures the redshift or blueshift of the light absorbed as a result of the speed of the atoms along the “line-of-sight” of the laser. The fastest atoms have the greatest shift and appear at the edges of the profile; the slowest atoms are those that absorb at the center of the profile. Measurements were taken with the polarization vector of the photolysis radiation aligned parallel (red lines) and perpendicular (black lines) to the line-of-sight direction of the probe laser. Note that the shapes of the reagent H and product D atom profiles are very similar, although the D atoms have smaller shifts (they are moving slower). The lower panel shows the inferred displacement mechanism. Figure reproduced (adapted) with permission from ref 33 (copyright 1991 Royal Society of Chemistry).

an H atom:



The H atoms in this photodissociation process are generated with high translational energy, in excess of 150 kJ mol^{-1} , and their velocities are perpendicular to the polarization vector (ϵ) of the absorbed photons (because the electronic transition moment is perpendicular to the plane of the H_2S molecule). Doppler profiles measured looking perpendicularly to ϵ were doubly peaked, because the H atoms move toward and away from the “observer” (see Fig. 10). The Doppler profiles of the product deuterium atoms were measured and found to present very similar behavior. The D atoms tend to emerge with velocities parallel to those of the incident H atoms, that is, scattered forward (although moving more slowly to conserve momentum). This result was interpreted in terms of a displacement mechanism proceeding via a transition state structure that is approximately a trigonal bipyramid, reminiscent of an $\text{S}_{\text{N}}2$ inversion mechanism.

Since the earliest crossed-beam studies, it was recognized that measurement of the angular correlation between the reagent (\mathbf{k}) and product (\mathbf{k}') relative velocity vectors may provide considerable information about the mechanism of the reaction and ultimately the details of the PES. It was not until relatively recently, however, that the rich vein of information available in the product rotational angular momentum (J') polarization was fully realized. Case and Herschbach (34) pointed the way in 1975 in a seminal paper on the statistical theory of the angular momentum polarization in chemical reactions. That work was stimulated by progress in crossed-beam reactive scattering experiments that employed magnetic fields to separate the products according to their orientation or alignment. At the same time, measurements of the polarization of light from chemiluminescent reactions were also beginning to uncover subtle aspects of the reactive PES (35, 36). In a prescient paper a few years later, Case, McClelland, and Herschbach (37) recognized that “The wedding of lasers and molecular beams...may allow the polarization of individual vibration–rotation states to be measured as a function of the scattering angle.” It is only in the late 1990s that their foresight has become reality. The wedding to which they refer has blossomed into a happy and fruitful marriage with many progeny. In the following section, armed with the tools and concepts touched upon in section 7, we give a flavor of the detail that can be attained.

8.2. Recent Experiments from Our Laboratory

8.2.1. The Reaction of Chlorine with Methane: Reagent Alignment

The reaction of electronic ground-state chlorine atoms $\text{Cl}(^2\text{P}_{3/2})$ with CH_4 in its vibrational ground state (eq 13) is endothermic ($\Delta H_0^0 = +7.9 \text{ kJ mol}^{-1}$), with a considerable barrier to reaction (ca. 15 kJ mol^{-1}).



This reaction is the simplest example of the chlorination of alkanes that takes place in the upper atmosphere. It is the principal pathway by which chlorine atoms are removed from the ClO_x cycle that catalytically destroys ozone (38). The reaction shows deviation from Arrhenius behavior (see section 2) and the understanding of this is of considerable importance to atmospheric modeling. An investigation of the

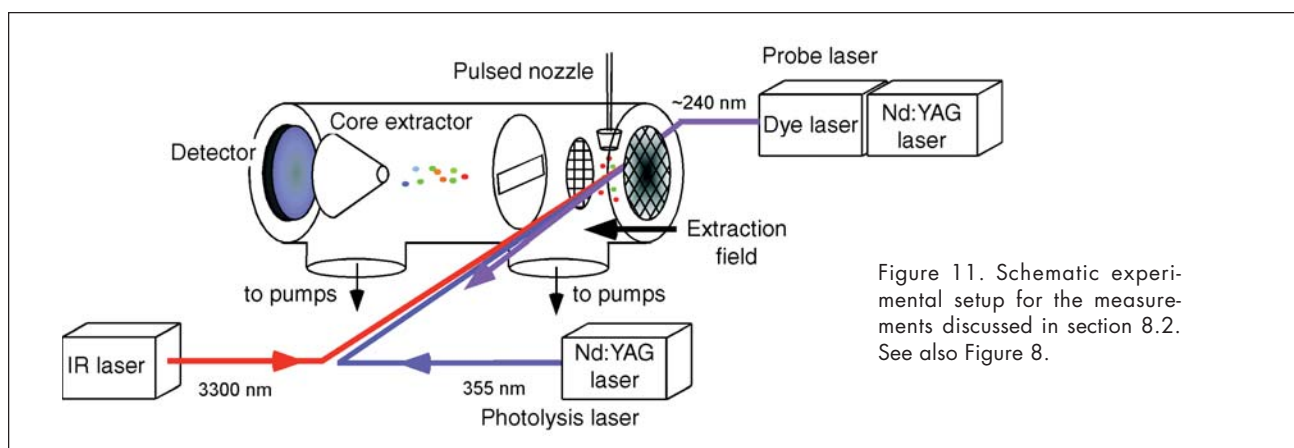


Figure 11. Schematic experimental setup for the measurements discussed in section 8.2. See also Figure 8.

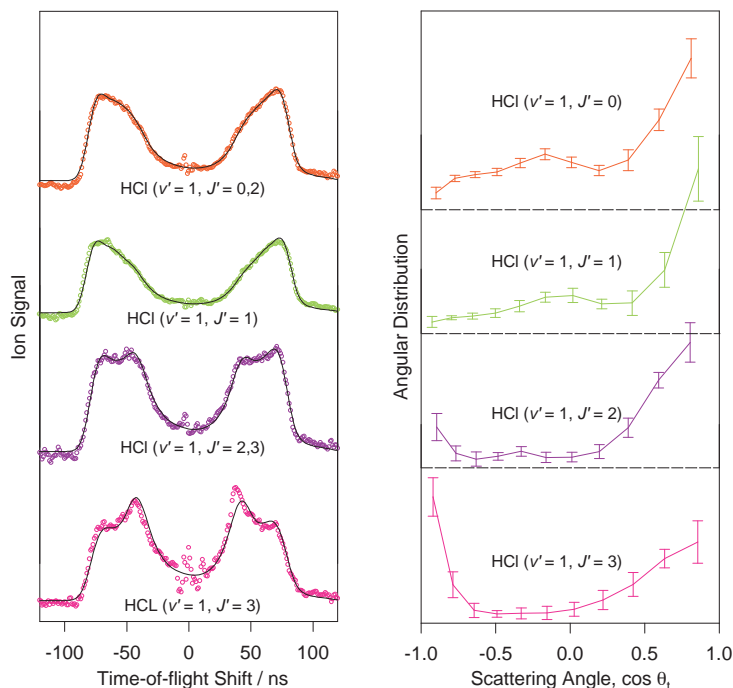
dynamics of the $\text{Cl} + \text{CH}_4$ system reveals a rich variation in the types of mechanism that contribute to the reaction.

A good photolytic source of Cl atoms is the 355-nm photolysis of Cl_2 , which produces almost exclusively (>98%) ground-state atoms observed to be highly spatially aligned (traveling in directions perpendicular to the polarization vector of the linearly polarized radiation). The collision energy between Cl and CH_4 at this wavelength is 15.3 kJ mol^{-1} , just above the reaction threshold, giving a somewhat low cross section, σ_R , for reaction. It is possible to increase the reactive cross section by increasing the collision energy of the reagents, which can be achieved by tuning the photolysis wavelength to higher energies (shorter wavelengths). A much more effective method of promoting the reaction, however, is vibrational excitation of the CH_4 , as shown by Simpson et al., who used infrared (IR) radiation to excite one quantum of the asymmetric stretch ($\nu_3 = 1$) of methane (29, 39). The two reagents, Cl_2 and CH_4 , were mixed in helium and expanded into a high vacuum via a pulsed nozzle (see Fig. 11). This expansion helped minimize the effects of thermal

averaging caused by the spread of reagent collision energies. An IR laser beam, tuned to excite the $0 \rightarrow 1$ vibrational transition of the ν_3 mode in CH_4 , was crossed perpendicular to the molecular expansion. The reaction was initiated by photolysis of Cl_2 using a second, linearly polarized ultraviolet laser beam that produced a velocity-aligned “pulse” of $\text{Cl}(^2P_{3/2})$ reagent atoms. Reaction products were allowed to build up for a few tens of nanoseconds, and the $\text{HCl}(v', J')$ products were interrogated with a third tunable laser pulse that selectively ionized the products from specific rovibrational states (v', J').

The velocity distribution of the HCl products was measured by recording the time of flight of the HCl^+ ions to a remote detector. Some results are shown in Figure 12. Analysis of these experimental results gave an extraordinarily detailed picture of the dynamics. HCl products generated in ($v' = 0$, high J') were scattered predominantly sideways (i.e., perpendicular to the velocity of the incoming Cl atom), with little dependence on the rotational state, J' . In contrast, the HCl molecules generated in ($v' = 1, J'$) were scattered predominantly forward for products with low rotation, but shifted

Figure 12. Example $\text{HCl}(v'=1, J')$ product TOF ion arrival profiles (left panel) and estimated scattering angular distributions (right panel). TOF shifts at the center (0) of the profiles correspond to slow HCl products, larger TOF shifts (at the edges) correspond to higher product HCl velocities (see Fig. 8). Circles are experimental data; solid lines are simulated fits of the data. Note the move from predominantly forward ($\cos \theta_i \rightarrow +1$) to backward scattering ($\cos \theta_i \rightarrow -1$) with increasing product rotation.



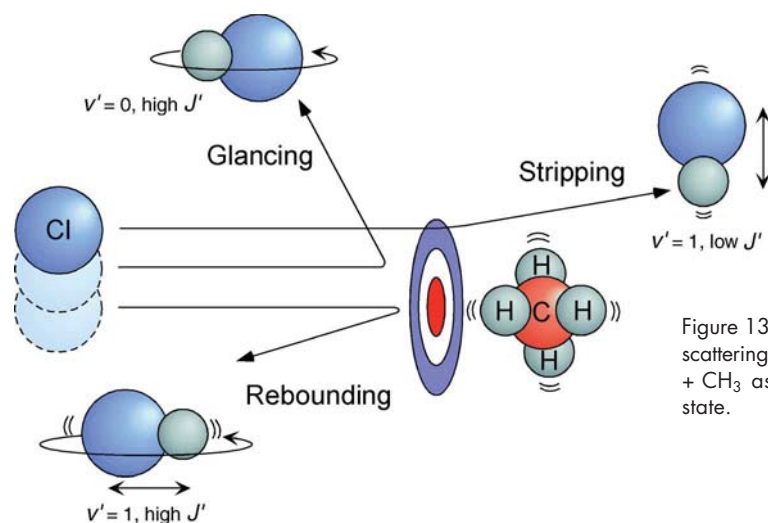


Figure 13. Scattering cartoon showing variation in product scattering for the reaction of $\text{Cl}(^2\text{P}_{3/2}) + \text{CH}_4 \rightarrow \text{HCl}(v', J') + \text{CH}_3$ as a function of $\text{HCl}(v', J')$ product rovibrational state.

toward the backward hemisphere with increasing product rotation. These findings are summarized in Figure 13. Very similar results were obtained when CD_3H was substituted for CH_4 , which suggests that the unobserved partner fragment (the CH_3 or CD_3) acts as a “spectator” (uninvolved bystander) through the reaction event.

The $\text{HCl}(v'=0)$ products were attributed to reaction via nearly head-on collisions of Cl with the H–C bond of methane, leading to sideways scattering. Forward-scattered products in $\text{HCl}(v'=1)$ were associated with peripheral or tangential collisions in which the H–C bond is pointing perpendicular to the velocity of the incoming Cl atom. These types of collision may be conveniently represented in false-color impact parameter (bull’s-eye) plots, as shown in Figure 14 (40). In these plots the CH_4 is the bull’s-eye of a dartboard and the concentric rings indicate how much scattering is estimated to come from peripheral or head-on collisions, corresponding to the edge or center of the dartboard, respectively. Darker rings indicate more reactive collisions at a particular radius on the dartboard. Figure 14c implies that $\text{HCl}(v'=1)$ products originate mostly from peripheral collisions.

The notion of reaction mechanisms involving either head-on or tangential collisions was confirmed by using polarized IR laser radiation to pre-align the H–C bond axis

through excitation of the ν_1 symmetric C–H stretch mode of the CD_3H molecule. The polarization of the photolysis laser was used to control the direction of the velocity-aligned Cl atoms with respect to pre-aligned H–C bond (39).

Simpson et al. also observed that, overall, vibrational excitation of the methane enhanced the reactive cross section (σ_R) by a factor of 30 (40). The enhancement in σ_R represents a dramatic increase in reactivity and can be attributed to a barrier that is quite “late” in the reaction pathway. A late barrier occurs where the collision transition state Cl-H-CH_3 looks more like the products than like the reagents: the reaction is encouraged by stretching the H– CH_3 bond. Indeed, this picture is consistent with the large enhancement of the reactive cross section with methane vibrational excitation. An “early” barrier would have a transition state that looks more like the reagents than the products (e.g., Cl-H-CH_3). The concept of late or early barriers is illustrated in Figure 15.

The quantum-state-resolved scattering measurements vividly illustrate the broad range of reactive collision mechanisms that go together to make a single reaction. The results show detail that would have been washed out if the HCl products had not been resolved into the angular scattering distributions of individual rovibrational states, detail that is generally beyond that obtained from traditional crossed molecular-beam studies as discussed in section 6.

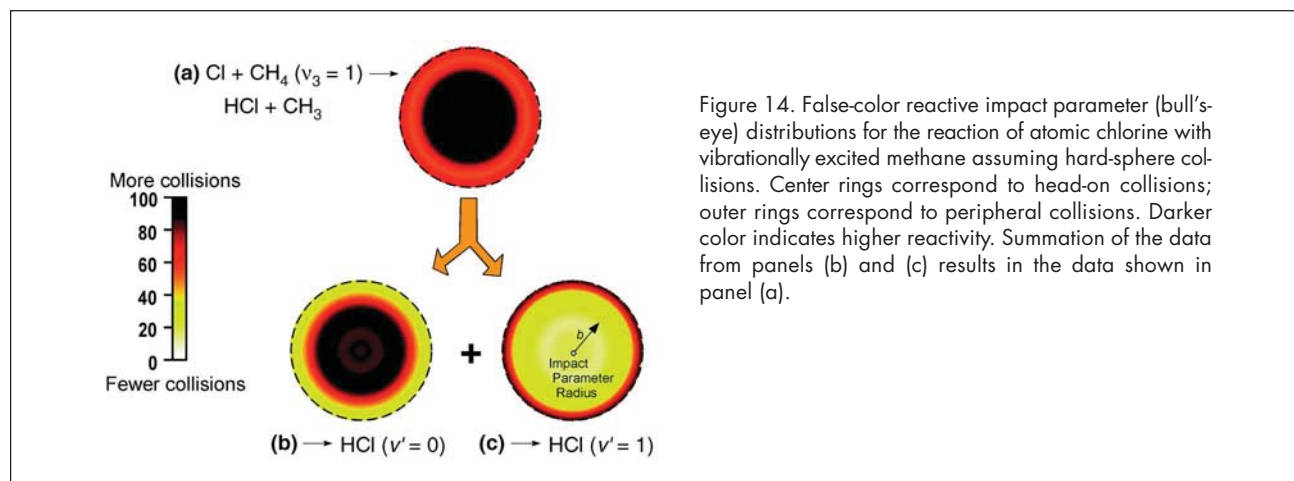


Figure 14. False-color reactive impact parameter (bull’s-eye) distributions for the reaction of atomic chlorine with vibrationally excited methane assuming hard-sphere collisions. Center rings correspond to head-on collisions; outer rings correspond to peripheral collisions. Darker color indicates higher reactivity. Summation of the data from panels (b) and (c) results in the data shown in panel (a).

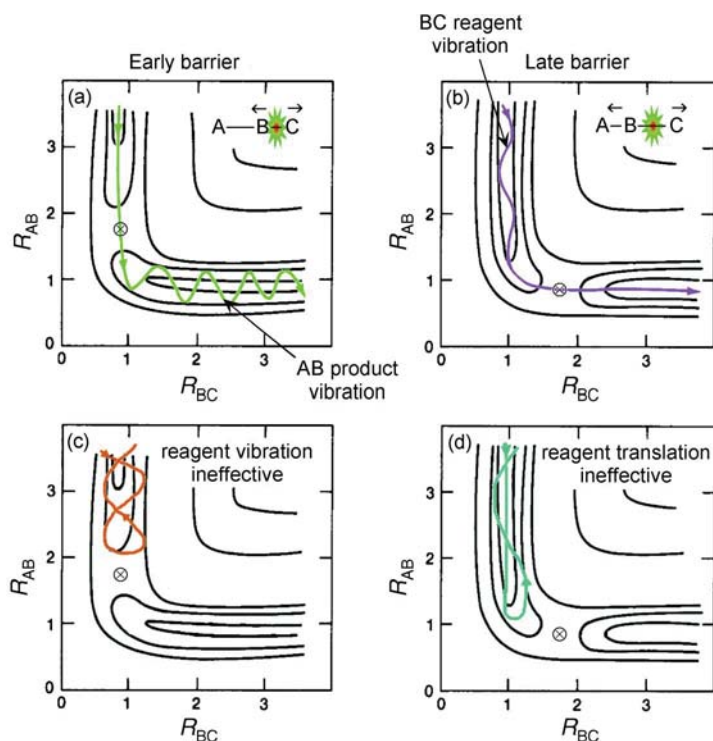


Figure 15. PESs for the reaction $A + BC \rightarrow AB + C$ showing the concept of early barriers (a and c) and late barriers (b and d). R_{AB} and R_{BC} are the AB and BC bond lengths, respectively. The saddle points are shown as points \otimes . For an early barrier the saddle point occurs in the reagent valley; for a late barrier the saddle point occurs in the product valley. Vibration in diatomic fragments produces “wiggles” in the trajectories, as shown.

For an early barrier, reagent translation is effective at surmounting the barrier (a), whereas reagent vibration is not effective (c). For the successful reaction shown in (a), energy is released when the AB bond is longer than the BC bond causing vibration in the product AB molecule.

For a late barrier, reagent vibration allows the trajectory to “cut the corner” to surmount the barrier (b), as is observed for the $\text{Cl} + \text{CH}_4$ reaction. Reagent translation causes the trajectory to be bounced back along the reagent valley (d). For the successful reaction shown in (b), energy is released when the BC bond is stretched compared to the AB bond, and most of the energy is released as relative translation of the AB + C products. Figure adapted from ref 3.

8.2.2. The Reaction of Chlorine with Methane: Product Alignment

In the previous section, we showed how polarized light can be used to explore the *reagent* alignment and how this can give us clues to determining the mechanisms that reactions follow. In particular, for the $\text{Cl} + \text{CH}_4$ reaction, the experimental clues suggest the existence of a *late barrier* in the reactive PES. In this final section, we show how observation of *product* alignment provides further evidence for the presence of a late barrier for this system.

As in the case of $\text{Cl}(^2P_{3/2}) + \text{CH}_4$, the reaction of chlorine atoms with *deuterated* methane (eq 14) is endothermic ($\Delta H_0^0 = +11.3 \text{ kJ mol}^{-1}$), with an activation energy estimated to be 16.3 kJ mol^{-1} :



The experimental setup used to study the alignment of the product rotational vector \mathbf{J}' was similar to that shown in Figure 11. The reaction is initiated by a linearly polarized laser

pulse at 303.5 nm that photolyzes Cl_2 molecules, producing an aligned pulse of fast $\text{Cl}(^2P_{3/2})$ atoms. The particular photolysis wavelength used gives the $\text{Cl} + \text{CD}_4$ reaction a collision energy of 27 kJ mol^{-1} . In contrast to the previous example, no IR laser pulse is used, and therefore the majority of the CD_4 molecules are in their vibrational ground state. Reaction products build up for 100 ns, and the resulting DCl molecules are ionized specifically from ($v'=0, J'=1$) states, by use of a second (linearly polarized) laser tuned to 241.1 nm.

How can we measure the preferential alignment, if any, of the product molecule? The absorption of linearly polarized light by a molecule depends on the transition dipole moment ($\boldsymbol{\mu}$) of the molecule, which is fixed with respect to the molecular axis. The absorption is maximal when the polarization vector of the light, $\boldsymbol{\epsilon}$, is parallel to $\boldsymbol{\mu}$. Because the rotational angular momentum, \mathbf{J}' , is also well defined with respect to the molecular axis, it is clear that the absorption of linearly polarized light will depend on the position of \mathbf{J}' with respect to $\boldsymbol{\epsilon}$ (see Fig. 16).

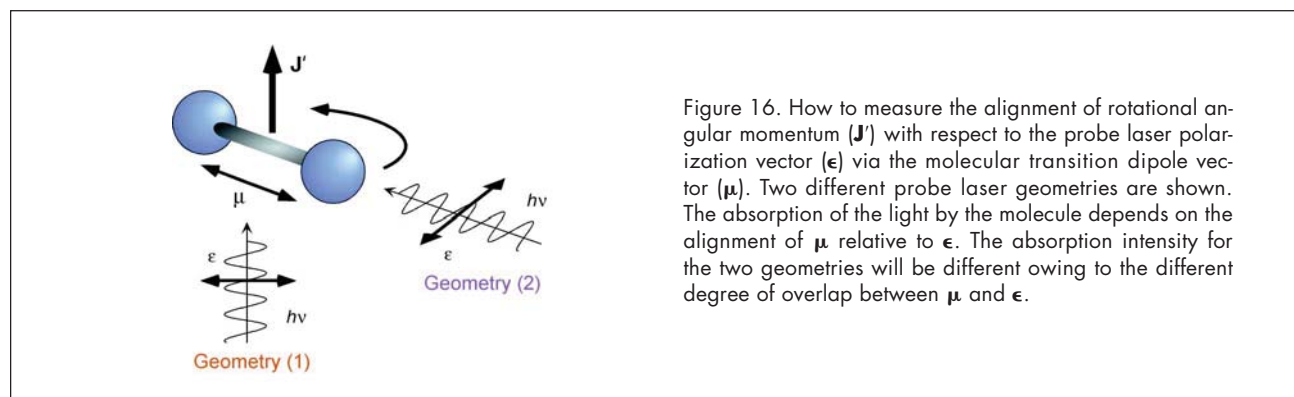


Figure 16. How to measure the alignment of rotational angular momentum (\mathbf{J}') with respect to the probe laser polarization vector ($\boldsymbol{\epsilon}$) via the molecular transition dipole vector ($\boldsymbol{\mu}$). Two different probe laser geometries are shown. The absorption of the light by the molecule depends on the alignment of $\boldsymbol{\mu}$ relative to $\boldsymbol{\epsilon}$. The absorption intensity for the two geometries will be different owing to the different degree of overlap between $\boldsymbol{\mu}$ and $\boldsymbol{\epsilon}$.

The amount of product DCl ionized in the probe ionization step depends on the alignment of \mathbf{J}' with respect to $\boldsymbol{\epsilon}$. The core-extraction TOF method detects only molecules with velocities parallel (and antiparallel) to the TOF axis (Fig. 8). By aligning $\boldsymbol{\epsilon}$ of the probe laser either parallel or perpendicular to the TOF axis, we can measure the alignment of \mathbf{J}' with respect to the velocity of the products.

Figure 17a shows a TOF profile that is sensitive to the product speed distribution. Figure 17b shows a TOF profile that is sensitive to the *alignment* of \mathbf{J}' as a function of the speed (and therefore the scattering angle) of the products. This trace has a more complicated shape, which we discuss below.

The TOF speed-dependent profile (Fig. 17a) was analyzed to give the angular distribution of $\text{HCl}(v'=0, J'=1)$ products scattered in the CM frame—that is, the correlation between \mathbf{k} and \mathbf{k}' . The products show an overall preference for backward scattering. The scattering can be quite well approximated assuming a hard-sphere scattering model, similar to the one mentioned in section 3, and consistent with the results shown in section 8.2.1.

The shape of the alignment-dependent profile, shown in Figure 17b, is very interesting, and is obtained by virtue of its being a *difference* between two ion-arrival profiles, recorded with the probe laser polarization parallel and perpendicular to the TOF axis, respectively. By simulating this difference form, Rakitzis et al. (41) determined a mechanism whereby \mathbf{J}' is maximally aligned preferentially perpendicular to the CM velocity of the product, \mathbf{u}_{DCl} (see Fig. 18).

The observed preference for $\mathbf{J}' \perp \mathbf{u}_{\text{DCl}}$ gives another subtle yet highly sophisticated clue to the precise mechanism of the reaction. From the previous section, we obtained a picture of the reaction where the light D (or H) atom is transferred directly to the Cl atom in a hard-sphere collision. The strong correlation of \mathbf{J}' to the *exit* velocity vector so that \mathbf{J}' points perpendicular to it is consistent with the picture that we developed in section 8.2.1, that the rotation of the product is determined *late* in the reactive collision sequence as the product is exiting from the transition state. The results give powerful evidence for the nature of the sequence of events in a reactive collision.

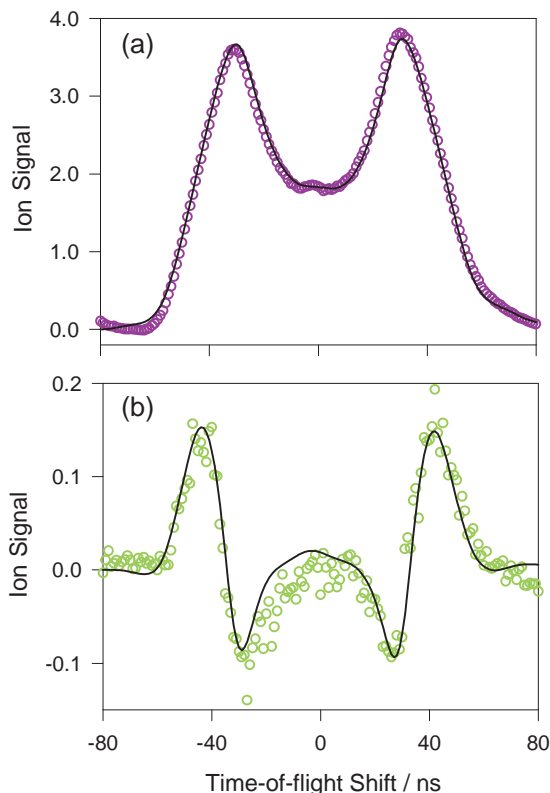
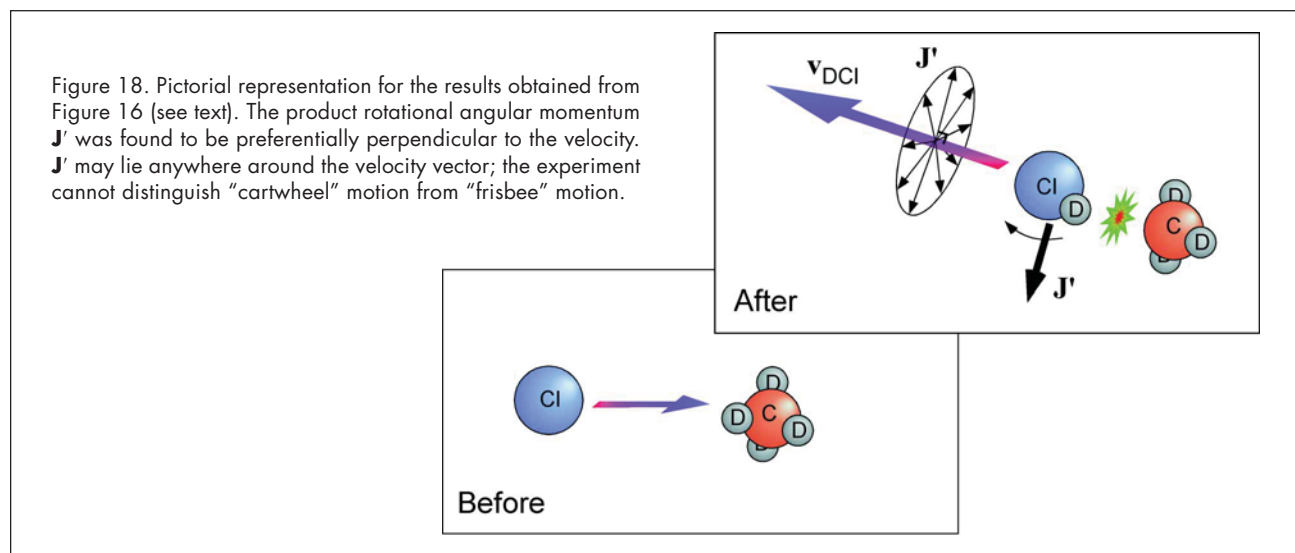


Figure 17. Composite $\text{DCl}(v'=0, J'=1)$ ion arrival profiles for the reaction of Cl with CD_4 . Experimental traces are shown as colored circles; the simulated fits are shown as solid lines. Two ion arrival traces were measured in different experimental geometries. The profile shown in (a) is a sum of the two measured traces, and (b) represents their difference. Profile (a) is dependent only upon product speed, whereas (b) is dependent on the alignment of product \mathbf{J}' as a function of product speed.





9. To the Future

So far in this overview, we have attempted to give a brief glimpse of the highly specific details of a reactive collision that can be obtained experimentally and a taste of the sophistication of these methods. In our final section, we speculate about the future and what it may hold for our understanding of reaction dynamics.

Powered by advances in laser techniques, the anatomies of elementary chemical reactions are being laid bare, both by direct time-resolved measurements and by skillful before-and-after detective work. At the same time, advances in computational chemistry are making it possible to determine the full description of a chemical reaction to a level of detail limited only by quantum mechanics (the uncertainty principle). Thus, the day is approaching when chemists can finally state that some simple elementary reactions are fully understood. Yet clouds remain in the sky. The major cloud is our faithful friend the Born–Oppenheimer approximation, which has served us so well in describing the spectroscopy of molecules close to their equilibrium configurations. Recall that it is this Born–Oppenheimer approximation that allows us to visualize reactions in mechanical terms as nuclear masses moving on a single multidimensional sur-

face that connects reactants to products. Unlike equilibrium geometries, reactions explore nuclear configurations in which more than one Born–Oppenheimer surface is present. This behavior is not abnormal but rather the rule, because in almost all reactions the reactants or the products, or both, involve electronically open-shell systems having fine-structure splittings. Consequently, it is possible for the reaction to be influenced by the proximity of other potential energy surfaces, even if the reaction does not access them.

A vital question remains unanswered. How important is the presence of these close potential energy surfaces, some of which intersect and some of which do not? As in the past, chemists will not be satisfied that they know the answer to this question until theory has advanced to the level that it can reliably predict such collision outcomes, and theory cannot be trusted without being underpinned by substantive, detailed experimental measurements.

It seems that reaction dynamics is no longer a child but rather a teenager, needing much attention. As this field matures, much still remains to be discovered about how elementary reactions occur.

Acknowledgments

We would like to thank S. Alex Kandel and T. Peter Rakitzis for their assistance in the preparation of this manuscript. This work has been supported by the National Science Foundation under grant CHE-93-22690.

Literature Cited

- McQuarrie, D. A.; Simon, J. D. *Physical Chemistry: A Molecular Approach*; University Science: Sausalito, CA, 1997.
- Atkins, P. W. *Physical Chemistry*, 6th ed.; Oxford University Press: New York, 1998.
- Levine, R. D.; Bernstein, R. B. *Molecular Reaction Dynamics and Chemical Reactivity*; Oxford University Press: New York, 1987.
- Smith, I. W. M. *Kinetics and Dynamics of Elementary Gas Reactions*; Butterworths: London, 1980.
- Steinfeld, J. I.; Francisco, J. S.; Hase, W. L. *Chemical Kinetics and Dynamics*, 2nd ed.; Prentice Hall: Englewood Cliffs, NJ, 1998.
- Nobel Laureates in Chemistry 1901–1992*; James, L. K., Ed.; American Chemical Society: Washington, DC, 1993.
- Arrhenius, S. *Z. Physik. Chem.* **1889**, *4*, 226.
- Lewis, W. C. McC. *J. Chem. Soc.* **1918**, *113*, 471.
- Laidler, K. J. *Chemical Kinetics*, 3rd ed.; HarperCollins: New York, 1987.
- Smith, I. W. M. *J. Chem. Educ.* **1982**, *59*, 9.
- The Journal of Chemical Education Software has available two Macintosh programs that show molecular collisions and trajectories over PESs. More details are available at http://jchemed.chem.wisc.edu/JCESoft/Issues/Series_C.
- Hirschfelder, J. O.; Eyring, H.; Topley, B. *J. Chem. Phys.* **1936**, *4*, 170.
- Eyring, H.; Polanyi, M. *Z. Phys. Chem.* **1931**, *B12*, 279.
- Bernstein, R. B.; Zare, R. N. *Phys. Today* **1980**, *33*, 43.
- Zewail, A. H.; Bernstein, R. B. In *The Chemical Bond: Structure and Dynamics*; Zewail, A. H., Ed.; Academic: San Diego, 1992; pp 223–279.
- Zewail, A. H. *Femtochemistry: Ultrafast Dynamics of the Chemical Bond*; World Scientific: Singapore, 1994.
- Shank, C. V. *Science* **1986**, *233*, 1276.
- Rose, T. S.; Rosker, M. J.; Zewail, A. H. *J. Chem. Phys.* **1989**, *91*, 7415.
- Polanyi, J. C. *Science* **1987**, *236*, 680.
- Neumark, D. M.; Wodtke, A. M.; Robinson, G. N.; Hayden, C. C.; Lee, Y. T. *J. Chem. Phys.* **1985**, *82*, 3045.
- Bull, T. H.; Moon, P. B. *Discuss. Faraday Soc.* **1954**, *17*, 54.
- Taylor, E. H.; Datz, S. *J. Chem. Phys.* **1955**, *23*, 1711.
- Herschbach, D. R. *Angew. Chem., Int. Ed. Engl.* **1987**, *26*, 1221.
- Lee, Y. T. *Science* **1987**, *236*, 793.
- Manolopoulos, D. E.; Stark, K.; Werner, H.-J.; Arnold, D. W.; Bradforth, S. E.; Neumark, D. M. *Science* **1993**, *262*, 1852.
- Manolopoulos, D. E. *J. Chem. Soc. Faraday Trans.* **1997**, *93*, 673.
- Norrish, R. W. G.; Porter, G. *Nature* **1949**, *164*, 658.
- Simpson, W. R.; Orr-Ewing, A. J.; Kandel, S. A.; Rakitzis, T. P.; Zare, R. N. *J. Chem. Phys.* **1995**, *103*, 7299.
- Simpson, W. R.; Orr-Ewing, A. J.; Zare, R. N. *Chem. Phys. Lett.* **1993**, *212*, 163.
- Aoiz, F. J.; Brouard, M.; Enriquez, P. A.; Sayos, R. *J. Chem. Soc. Faraday Trans.* **1993**, *89*, 1427.

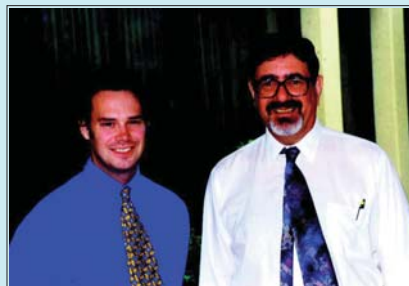
31. Brouard, M.; Simons J. P. In *The Chemical Dynamics and Kinetics of Small Radicals*; Liu, K.; Wagner, A., Eds.; World Scientific: Singapore, 1995; pp 795–841.
32. Orr-Ewing, A. J.; Zare, R. N. In *The Chemical Dynamics and Kinetics of Small Radicals*; Liu, K.; Wagner, A., Eds.; World Scientific: Singapore, 1995; pp 936–1063.
33. Katz, B.; Park, J.; Satyapal, S.; Tasaki, S.; Chattopadhyay, A.; Yi, W.; Bersohn, R. *Faraday Discuss. Chem. Soc.* **1991**, *91*, 73.
34. Case, D. A.; Herschbach, D. R. *Mol. Phys.* **1975**, *30*, 1537.
35. van Brunt, R. J.; Zare, R. N. *J. Chem. Phys.* **1968**, *48*, 4304.
36. Chamberlain, G. A.; Simons, J. P. *J. Chem. Soc. Faraday Trans. 2* **1975**, *71*, 2043.
37. Case, D. A.; McClelland, G. M.; Herschbach, D. R. *Mol. Phys.* **1978**, *35*, 541.
38. Wayne, R. P. *Chemistry of Atmospheres: An Introduction to the Chemistry of the Atmospheres of Earth, the Planets, and Their Satellites*, 2nd ed.; Oxford University Press: London, 1991.
39. Simpson, W. R.; Orr-Ewing, A. J.; Kandel, S. A.; Rakitzis, T. P.; Zare, R. N. *J. Chem. Phys.* **1995**, *103*, 7313.
40. Simpson, W. R.; Rakitzis, T. P.; Kandel, S. A.; Lev-On, T.; Zare, R. N. *J. Phys. Chem.* **1996**, *100*, 7940.
41. Rakitzis, T. P.; Kandel, S. A.; Lev-On, T.; Zare, R. N. *J. Chem. Phys.* **1997**, *107*, 9392.

Viewpoints: Chemists on Chemistry

Anatomy of Elementary Chemical Reactions

Andrew J. Alexander and Richard N. Zare

Department of Chemistry, Stanford University,
Stanford, CA 94305-5080



Andrew J. Alexander

Department of Chemistry, Stanford University,
Stanford, CA 94305
email: andrewa@leland.stanford.edu

D.Phil., Physical Chemistry, 1997, Oxford University
B.Sc., Chemical Physics, 1994, Edinburgh University

Andrew J. Alexander obtained his B.Sc. in Chemical Physics (1994) from Edinburgh University and his D.Phil in Physical Chemistry (1997) from Oxford University under the supervision of John Simons. Alexander is presently a postdoctoral research associate in Richard Zare's group in the chemistry department at Stanford University where he is working on fundamental studies of reaction dynamics using lasers and mass spectrometry.

Richard N. Zare

Department of Chemistry, Stanford University,
Stanford, CA 94305
email: zare@stanford.edu

Ph.D., Chemical Physics, 1964, Harvard University
B.A., Chemistry and Physics, 1961, Harvard University

Richard N. Zare is renowned for his research in the area of laser chemistry, resulting in a greater understanding of chemical reactions at the molecular level. His sphere of expertise encompasses a wide range of disciplines ranging from reaction dynamics to analytical chemistry. Zare is currently the Marguerite Blake Wilbur Professor in Natural Science at Stanford University. He has been the recipient of numerous honors and awards resulting from his many significant contributions to chemistry, including the National Medal of Science (1983). His commitment to education is equally visible: he has presented invited lectures and seminars at many institutions around the world and was awarded the Bing Fellowship Award for Excellence in Teaching from Stanford University (1996). Zare has recently completed a two year term as chairman of the National Science Board (NSB).